Supplementary Material for

Earthquake nucleation and triggering on an optimally oriented fault

Carl Tape, Michael West, Vipul Silwal, Natalia Ruppert

Earth and Planetary Science Letters

November 27, 2012

List of Figures

List of Tables

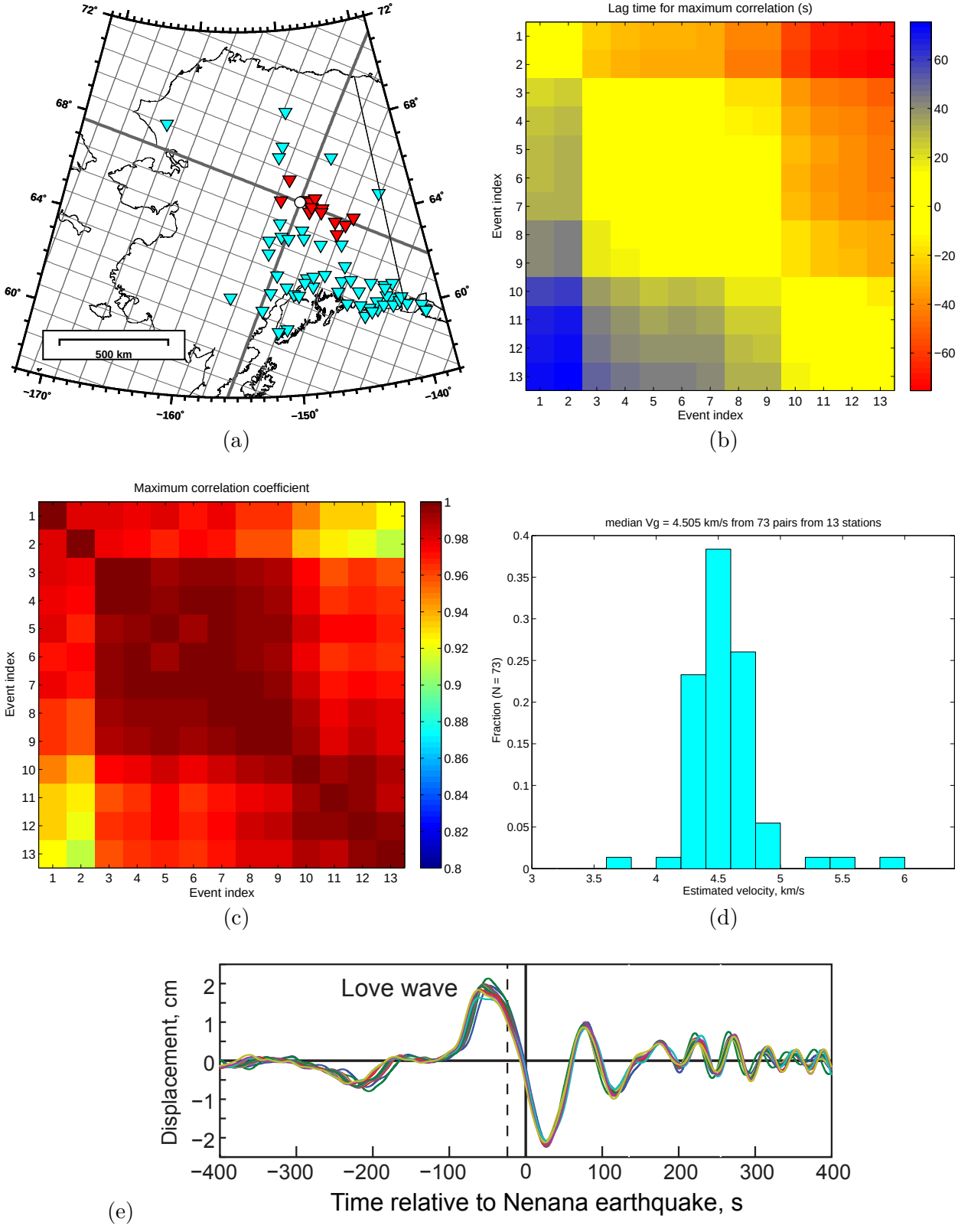

(a) (b) (c) (d) (e)

Figure S1: Procedure used for estimating the group velocity of the Sumatra Love wave recorded in central Alaska. (a) Station map highlighting the 13 stations (red) used in the cross correlation analysis to estimate the group velocity. These stations are a subset of the 79 total that are within 1° of the azimuthal angle of 22.3° from Sumatra to the Nenana. (b) Matrix of time lags between all station pairs. (c) Matrix of cross-correlation coefficients. (d) Histogram of estimated velocities from all station pairs. (e) Love waves from all 13 stations, time-shifted according to $V_g = 4.5$ km/s.

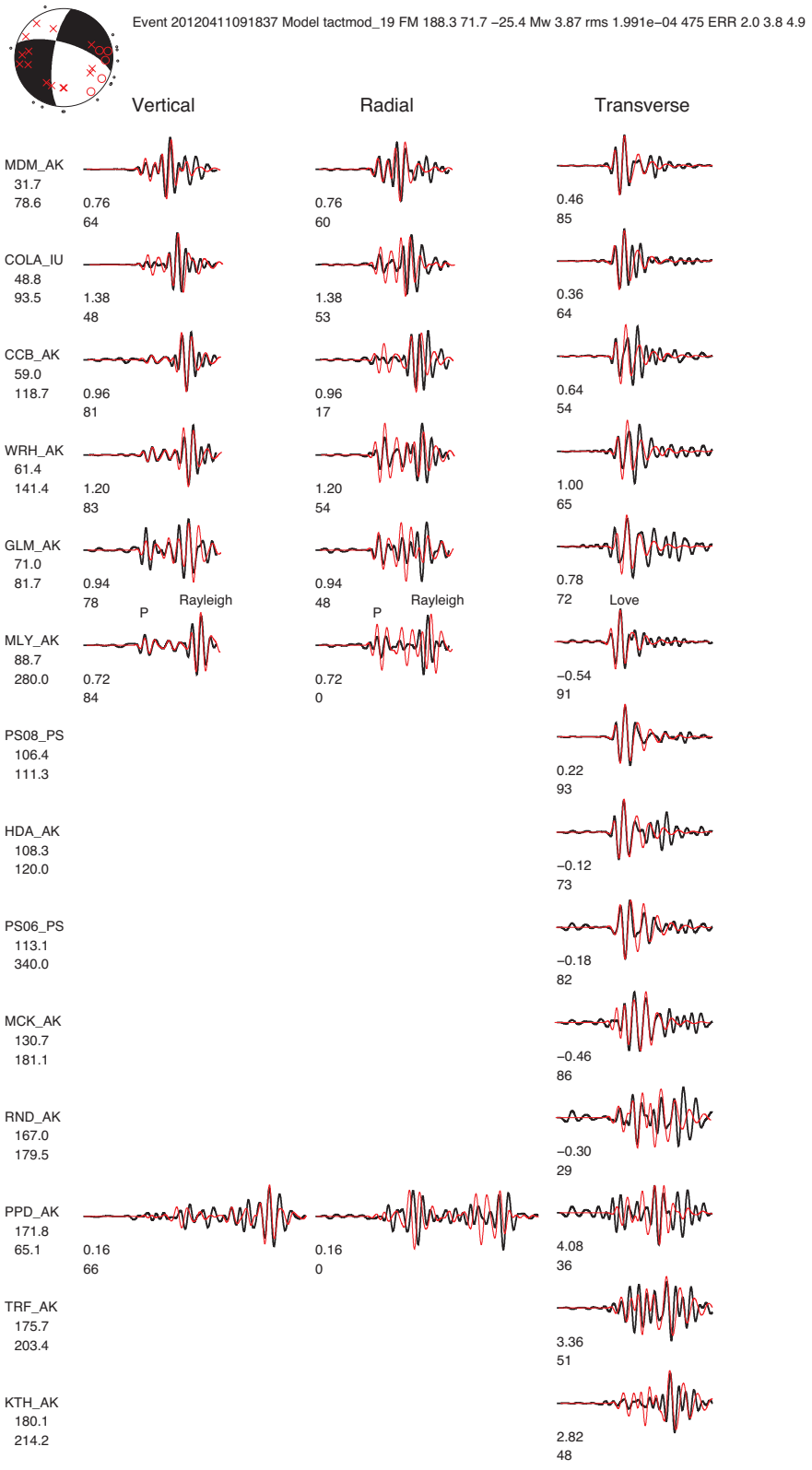

Figure S2: Focal mechanism inversion for the Nenana earthquake, using the method of *Zhu and Helmberger* (1996). Observed three-component seismograms (black) compared with synthetic seismograms (red), both filtered between 0.3 Hz and 0.6 Hz. Stations are ordered in increasing distance from the source. Synthetic seismograms are computed using a frequency-wavenumber method *Zhu and Rivera* (2002). Synthetic seismograms are time-shifted for maximal cross-correlation, which accounts for (some) unknown 3D structure (Figure S3a).

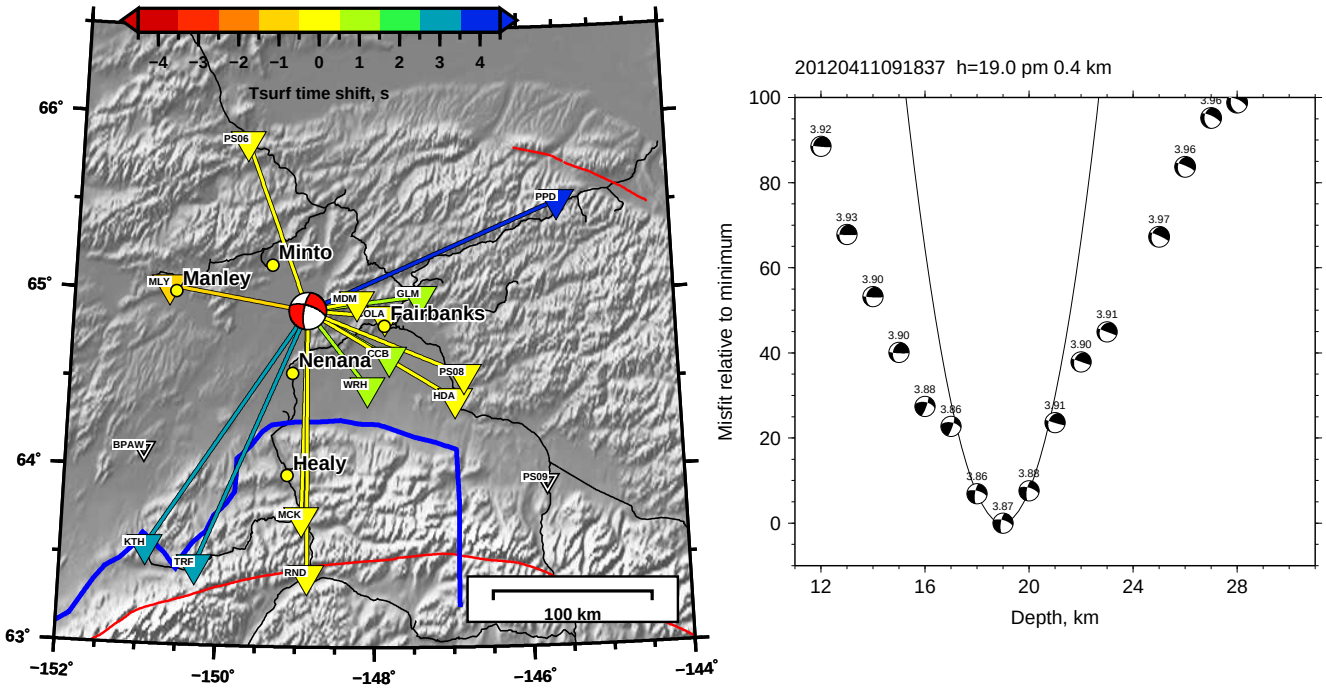

(a) **(b)**

Figure S3: Additional details on the focal mechanism inversion of the Nenana earthquake (Figure S2). **(a)** Love wave time shifts between observed seismograms and synthetic seismograms from a 1D model. The time shifts are labeled beneath the transverse component records in Figure S2. (Note: These are the Love waves from the Nenana earthquake that occur "within" the much longer period Love waves from the Sumatra earthquake.) The time shift convention is $\Delta t = t_{\text{obs}} - t_{\text{syn}}$ such that a positive time shift indicates that the synthetics arrive too soon, which implies that the 1D reference model is too fast for these paths. Similarity between nearby paths suggests that the time shifts indicate real structural differences, rather than clock errors or spurious measurements. **(b)** Grid search over depth to obtain the best estimate of 19 ± 0.4 km. If different depths are assumed, then both the magnitude and focal mechanism will generally change. The best-fitting parabola near the minimum is used to estimate the uncertainty for the depth estimate; clearly the misfit function is not quadratic far from the minimum.

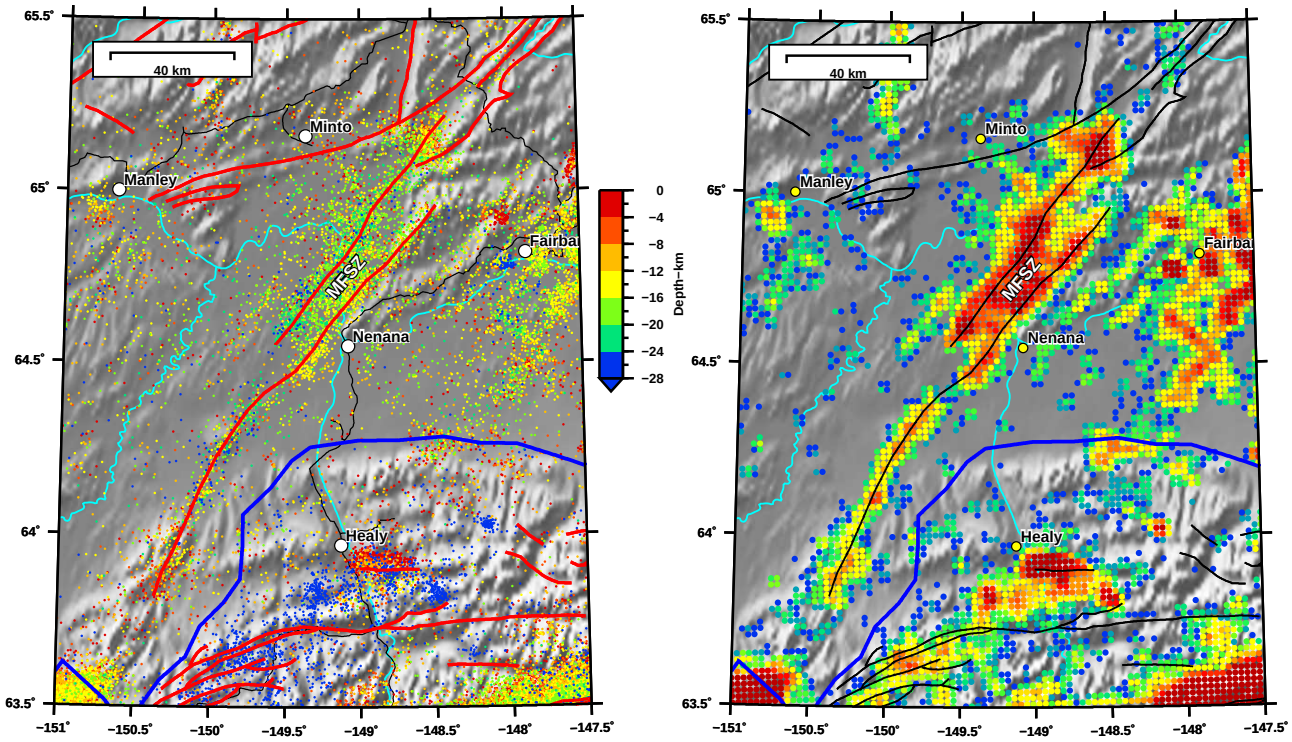

Figure S4: Inferring two faults from seismicity in the Minto Flats seismic zone. **(a)** Seismicity from the AEIC catalog, 1990–2010, $M > 0$. **(b)** Seismicity density from (a), plotted on a logarithmic color scale, which reveals the dominant two fault strands that we digitized. Other faults plotted are from (*Plafker et al.*, 1994). The Minto Flats seismic zone (MFSZ) has previously been described as a single, diffuse seismic zone that extends approximately 200 km from SW to NE (*Pulpan*, 1986; *Biswas and Tytgat*, 1988; *Page et al.*, 1995; *Ratchkovski and Hansen*, 2002). Despite the prominence of the two seismic lineaments, neither lineament appears as an active or inactive fault in the fault map of *Plafker et al.* (1994). The eastern lineament coincides with the Minto fault mapped by *Péwé et al.* (1966), but later interpreted as geomorphic feature (*Page et al.*, 1991; *Plafker et al.*, 1994). Here we suggest that the lineaments be identified as two active faults. The two faults of the MFSZ appear to bound the gravity-low signature of the Nenana sedimentary basin (*Barnes*, 1961; *Van Kooten et al.*, 2012).

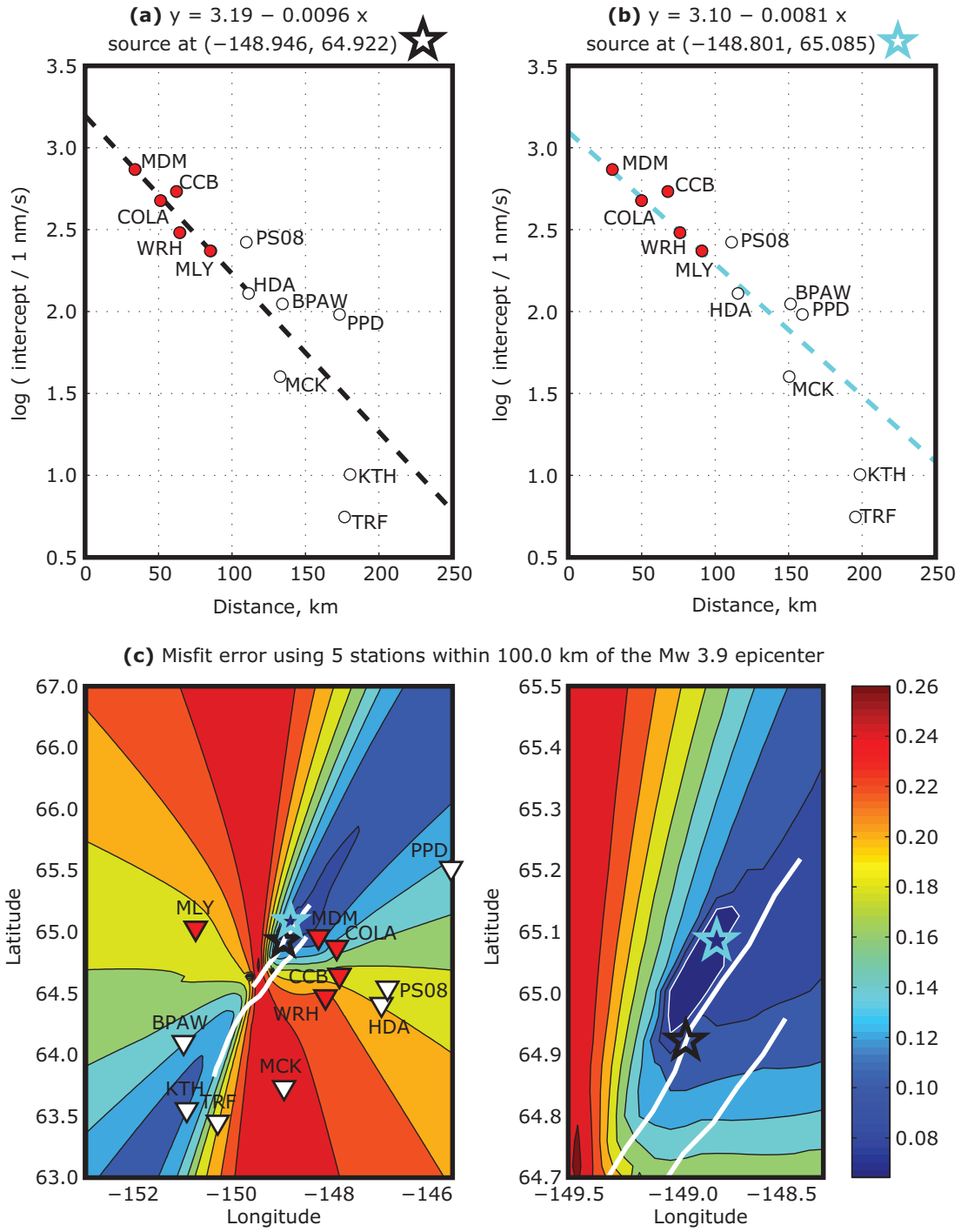

Figure S5: Estimating the location of the foreshock signal using a simple attenuation model, $A = A_0 e^{-kx}$, where x is the source-station distance. As shown in Figure 6, the log-scaled foreshock signal (vertical velocity filtered 2–8 Hz) can be represented by a best-fitting line with slope and intercept. The intercept corresponds to the amplitude of the foreshock signal immediately prior to the M_w 3.9 event. This amplitude decreases as a function of distance from the Nenana epicenter, as plotted in (a). We perform a grid search over possible locations using all five stations within 100 km of the Nenana epicenter. By searching the entire region for possible source locations for the foreshock signal (c), we obtain a minimum (cyan star) that is 19 km from the Nenana event; the fit to data is shown in (b) and is only slightly better than in (a) (0.06 vs 0.11). We hypothesize that the foreshock signal and the M_w 3.9 earthquake occur at the same place. This simple analysis does not refute our hypothesis. The line fitting was performed using the robust-fitting function `robustfit` in Matlab.

Table S1: Source parameters for the 2012 Nenana earthquake and a 2004 comparison earthquake. Fault angles are listed for both possible fault planes. Based on the tectonic setting, we interpret the first set of angles to be the fault plane. See also Figures S2 and S3. 'AEIC' denotes the AEIC earthquake catalog; 'AEIC-MT' denotes the AEIC moment tensor catalog (*Ratchkovski and Hansen*, 2002). Note that the AEIC moment tensor for the 2004 event also includes a non-double-couple component, which we do not represent in this table.

	2012-04-11 event		**2004-11-17 event**	
parameter	value	source	value	source
origin time	09:21:57.44	AEIC	11:29:00.34	AEIC
longitude	$-148.9461°$	AEIC	$-149.1049°$	AEIC
latitude	$64.9222°$	AEIC	$64.8872°$	AEIC
depth	19 km	this study	19 km	AEIC
M_0	8.1×10^{14} N m	this study	2.8×10^{14} N m	AEIC-MT
M_w	3.9	–	3.6	–
half-duration τ_h	0.22 s	$\left(2.4 \times 10^{-6}\right) M_0^{1/3}$	0.16 s	$\left(2.4 \times 10^{-6}\right) M_0^{1/3}$
strike-1	$188.3°$	this study	$188.8°$	AEIC-MT
dip-1	$71.7°$	this study	$41.1°$	AEIC-MT
rake-1	$-25.4°$	this study	$-23.7°$	AEIC-MT
strike-2	$286.8°$	—	$297.2°$	–
dip-2	$66.0°$	—	$74.7°$	–
rake-2	$-159.9°$	—	$-128.6°$	–

References

Barnes, D. F. (1961), Gravity low at Minto flats, in *Short Papers in the Geologic and Hydrologic Sciences, Articles 293–435: Geological Survey Research 1961*, pp. D254–D257, U.S. Geol. Survey, Washington, D.C., Professional Paper 424-D.

Biswas, N. N., and G. Tytgat (1988), Intraplate seismicity in Alaska, *Seis. Res. Lett.*, *59*(4), 227–233.

Page, R. A., N. N. Biswas, J. C. Lahr, and H. Pulpan (1991), Seismicity of continental Alaska, in *Neotectonics of North America*, edited by D. B. Slemmons, E. R. Engdahl, M. D. Zoback, and D. D. Blackwell, The Geology of North America, chap. 4, Geol. Soc. Am., Boulder, Colo., USA, Decade Map Volume 1.

Page, R. A., G. Plafker, and H. Pulpan (1995), Block rotation in east-central Alaska: A framework for evaluating earthquake potential?, *Geology*, *23*(7), 629–632.

Péwé, T. L., C. Wahrhaftig, and F. R. Weber (1966), Geologic Map of the Fairbanks Quadrangle, U.S. Geol. Survey Miscellaneous Investigation Series I-455.

Plafker, G., L. M. Gilpin, and J. C. Lahr (1994), Neotectonic Map of Alaska, in *Geology of Alaska*, *The Geology of North America*, vol. G-1, edited by G. Plafker and H. C. Berg, Geol. Soc. Am., Boulder, Colo., USA, Plate 12.

Pulpan, H. (1986), Seismic-Hazard Analysis of the Nenana Agricultural Development Area, Central Alaska, Alaska Division of Geological and Geophysical Surveys Public-data File 86–78.

Ratchkovski, N. A., and R. A. Hansen (2002), New constrains on tectonics of interior Alaska: Earthquake locations, source mechanisms, and stress regime, *Bull. Seis. Soc. Am.*, *92*(3), 998–1014.

Van Kooten, G. K., M. Richter, and P. A. Zippi (2012), Alaska's Interior rift basins: a new frontier for discovery, *Oil & Gas J.*, *110*(1a), 10 p.

Zhu, L., and D. Helmberger (1996), Advancement in source estimation techniques using broadband regional seismograms, *Bull. Seis. Soc. Am.*, *86*(5), 1634–1641.

Zhu, L., and L. A. Rivera (2002), A note on the dynamic and static displacements from a point source in multilayered media, *Geophys. J. Int.*, *148*, 619–627.